EVOLUTIONARY BIOLOGY

Developmental basis of evolutionary lung loss in plethodontid salamanders

Zachary R. Lewis[1]†, Ryan Kerney[2], James Hanken[1]*

One or more members of four living amphibian clades have independently dispensed with pulmonary respiration and lack lungs, but little is known of the developmental basis of lung loss in any taxon. We use morphological, molecular, and experimental approaches to examine the Plethodontidae, a dominant family of salamanders, all of which are lungless as adults. We confirm an early anecdotal report that plethodontids complete early stages of lung morphogenesis: Transient embryonic lung primordia form but regress by apoptosis before hatching. Initiation of pulmonary development coincides with expression of the lung-specification gene *Wnt2b* in adjacent mesoderm, and the lung rudiment expresses pulmonary markers *Nkx2.1* and *Sox9*. Lung developmental-genetic pathways are at least partially conserved despite the absence of functional adult lungs for at least 25 and possibly exceeding 60 million years. Adult lung loss appears associated with altered expression of signaling molecules that mediate later stages of tracheal and pulmonary development.

INTRODUCTION

Vestigial structures provide a window into the evolutionary history of animals as well as the developmental mechanisms that underlie organ formation and loss (*1*–*3*). Darwin emphasized the importance of organ rudiments in providing compelling support for evolution by natural selection: "[rudimentary] organs may be compared with the letters in a word, still retained in the spelling, but become useless in the pronunciation, but which serve as a clue in seeking for its derivation" [(*4*), pp. 455–456]. Common examples are the transient limb buds and rudimentary pelvic girdles found in numerous tetrapods that have undergone limb loss (*3*, *5*). Vestiges of internal organs have received far less attention than those visible externally, likely because detailed anatomical characterization is necessary to observe them in the first place. However, internal organ rudiments have the potential to reveal how organ loss can occur in highly pleiotropic genetic networks and within tightly integrated developmental systems.

One instance of organ loss at the base of a major adaptive radiation is provided by the salamander family Plethodontidae (Fig. 1A). This is the most speciose family of salamanders; it accounts for more than two-thirds of extant salamander diversity (*6*). However, all adult plethodontids are lungless; they respire entirely through nonpulmonary tissues, mainly the skin and buccopharyngeal mucosa (*7*, *8*). Lung loss has occurred independently at least three additional times among distantly related amphibians, and other instances of lung reduction or loss are common among both amphibians and other vertebrates (Fig. 1A) (*1*, *9*–*11*). While the adaptive significance and ecological context of lung loss in plethodontids are highly debated (*12*, *13*), little is known about its developmental underpinnings (*14*).

The discovery of lunglessness in plethodontids in the late 19th century triggered the search for a vestigial lung (*15*, *16*). The most extensive study was by A. G. Mekeel, a doctoral student at Cornell University in the 1920s, who compared lung morphogenesis in the spotted salamander, *Ambystoma maculatum* (Ambystomatidae), to development in plethodontids. Although Mekeel (*17*) could find no trace of a lung, or even a glottis, in adult plethodontids, she describes in her dissertation incipient stages of lung development in embryos: A lung rudiment is present transiently but disappears before hatching. Unfortunately, except for a single conference abstract (*18*), Mekeel's research was never published and her work is largely forgotten. Moreover, researchers have largely neglected this phenomenon over the subsequent 90 years.

In this study, we evaluate, correct, and extend the initial morphological accounts of lung loss in plethodontids and explore their developmental and genetic correlates. We confirm that an incipient lung does form in embryos of several species; its morphological features closely resemble those seen in the axolotl, *Ambystoma mexicanum*, a lunged salamander in the family Ambystomatidae (*19*–*21*). These features are likely conserved since the plethodontid lineage diverged from other living salamander families more than 100 million years (Ma) ago (*22*) and despite subsequent lung loss. However, the lung anlage in plethodontids is only present transiently; it regresses by programmed cell death, or apoptosis, well before hatching. We also find characteristic embryonic expression of several genetic markers that are associated with lung development in the axolotl as well as other tetrapods—mesenchymal *Wnt2b* (*23*–*25*), endodermal *Nkx2.1* (*26*–*28*), and *Sox9* (*28*, *29*). Last, heterospecific grafting experiments involving lunged-salamander embryos suggest that in plethodontids, the foregut endoderm, one of two primary cell populations that contribute to the adult lung, is competent to respond to pulmonary inductive cues from adjacent mesoderm and extend the development of pulmonary diverticula beyond that achieved during normal development. Plethodontid salamanders, despite lacking any trace of lungs as adults, partially conserve as embryos the developmental-genetic pathways that mediate pulmonary development in vertebrates generally (*30*).

RESULTS

Lungless salamanders develop a lung rudiment

We analyzed developmental series of lungless salamanders (Plethodontidae) to determine whether a lung rudiment forms embryonically.

[1]Department of Organismic and Evolutionary Biology and Museum of Comparative Zoology, Harvard University, Cambridge, MA, USA. [2]Department of Biology, Gettysburg College, Gettysburg, PA, USA.
*Corresponding author. Email: hanken@oeb.harvard.edu
†Present address: NanoString Technologies, Seattle, WA, USA.

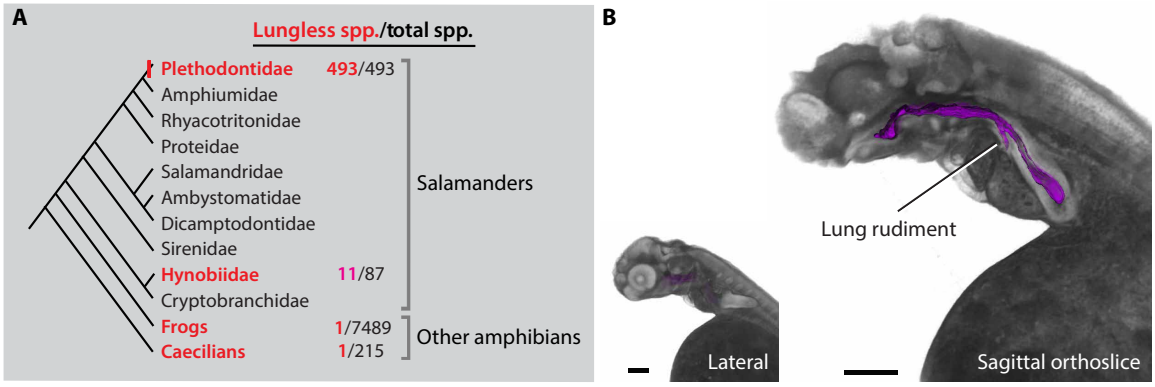

Fig. 1. All plethodontid salamanders are lungless as adults, but lungs begin to form in embryos. (**A**) Lungs have been lost independently at least four times among living amphibians (red font), but Plethodontidae is the only clade in which all species are lungless as adults. Cladogram and species numbers are from (*6*). (**B**) X-ray micro–computed tomography (μCT) scan of a *P. cinereus* embryo, stage *Pc18*, which has completed initial stages of lung formation. The sagittal orthoslice shows the lung rudiment [laryngotracheal tube (LT)] descending from the floor of the pharynx. Endoderm is shaded purple.

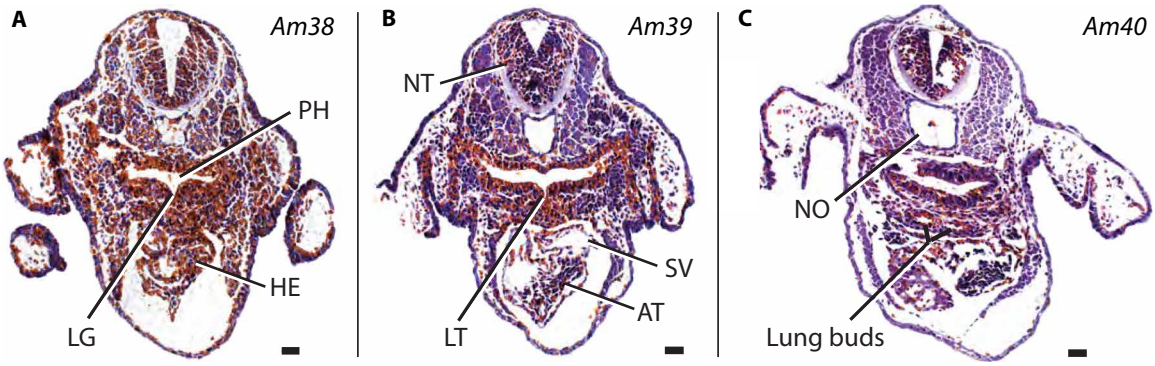

Fig. 2. Lung development in a lunged salamander, *A. mexicanum*. (**A**) Lung development begins by embryonic stage *Am38* with the appearance of a median laryngotracheal groove (LG) in the floor of the pharynx (PH). (**B**) The groove extends ventrally and caudally to form the LT at stage *Am39*. (**C**) Lung buds are visible in a more posterior section at stage *Am40*. Transverse sections; dorsal is at the top. AT, atrium; HE, heart; NO, notochord; NT, neural tube; SV, sinus venosus. Scale bars, 50 μm.

We focused primarily on *Plethodon cinereus*, the eastern red-backed salamander, a direct-developing species that lacks a free-living, aquatic larva (*31*, *32*). Additional series were prepared from two distantly related metamorphosing species, *Desmognathus fuscus*, the northern dusky salamander, and *Hemidactylium scutatum*, the four-toed salamander. These series were compared to embryos of *A. mexicanum*, the axolotl.

The first morphological sign of lung development in *A. mexicanum* is the formation at stage *Am38* of a median laryngotracheal groove (LG) in the ventral foregut (Figs. 2A and 3, A and B). This groove becomes a distinct diverticulum, the laryngotracheal tube (LT; or lung rudiment), which emerges during stage *Am39* from the ventral foregut dorsal to the heart at the axial level of the division between the sinus venosus and atrium (Fig. 2, A and B). The LT then elongates and bifurcates and becomes surrounded by lung mesenchyme by stage *Am40*, when lung buds are clearly visible at its caudal end (Figs. 2C and 3, E and F). Lung buds and trachea, the latter triangular in cross section, are further enlarged at stage *Am41* (Fig. 3G). The trachea is well developed by *Am43* and the glottis is distinct by *Am44* (hatching), when the lungs are simple saccular structures with walls approximately two cell layers thick (Fig. 3, H to J).

Similar morphogenetic events occur initially in lungless *P. cinereus*. An LG begins to form during stage *Pc17* and is clearly visible by early-stage *Pc18* (Fig. 4). By late-stage *Pc18*, the LT comprises a posteroventral diverticulum from the foregut, which has a lumen continuous with the pharynx (Figs. 1B and 5, A to D). The LT of *P. cinereus* resembles that of *A. mexicanum*; both feature a simple cuboidal epithelium surrounded by ventral mesenchyme (Figs. 3F and 5D). Likewise, at early stages in each species, the LT diverticulum is flattened ventrally and bears slight lateral flanges, which precede formation of paired lung buds (Figs. 3F and 5C). The LT appears less distinct in the mesolecithal egg of *A. mexicanum* because of the broad distribution of yolk platelets, which slightly obscure histological morphology at early stages. In the telolecithal egg of *P. cinereus*, the abundant yolk stores are instead sequestered in the endoderm, leaving the LT readily apparent.

The LT in *P. cinereus* continues to elongate through stage *Pc21*, when pulmonary development begins to diverge histologically from

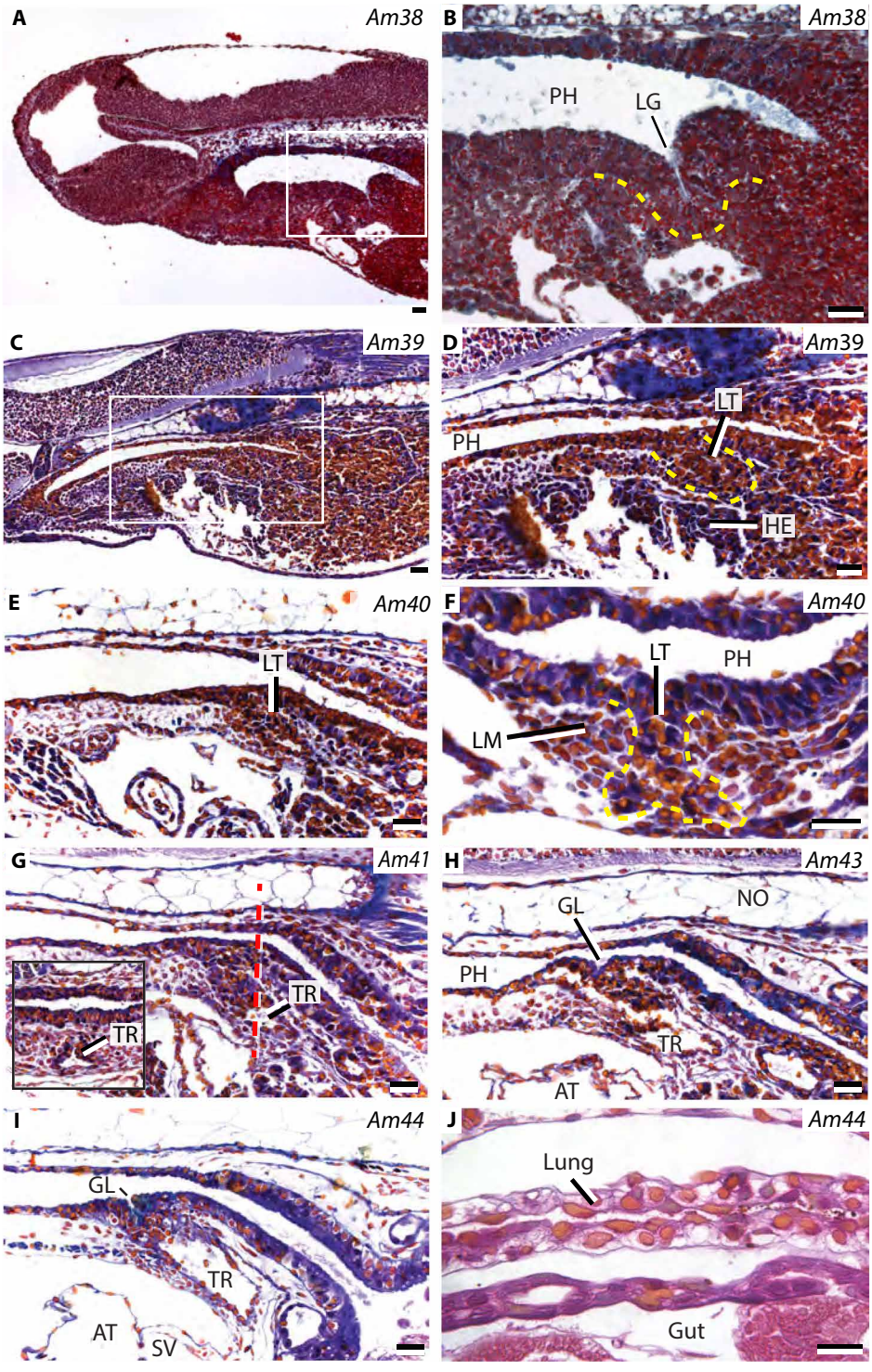

Fig. 3. Lung development in a lunged salamander, *A. mexicanum*. (**A** and **B**) The LG is visible in a midsagittal section through the head at stage *Am38*. Boxed area in (A) is enlarged in (B). (**C** and **D**) The groove extends ventrally and caudally to form the LT dorsal to the heart (HE) at stage *Am39*. Boxed area in (C) is enlarged in (D). (**E** and **F**) At stage *Am40*, the elongate and bifurcated LT is surrounded by lung mesenchyme (LM). (**G** and **H**) The developing trachea (TR) is surrounded by lung mesenchyme at stage *Am41* and is fully formed by stage *Am43*. Inset box in (G) depicts a transverse section at the axial level indicated by the red dashed line. (**I**) The glottis (GL), first detectable at stage *Am43*, is distinct by stage *Am44*. (**J**) Lungs are fully formed by hatching. (F) is a transverse section; other panels are midsagittal sections; anterior is to the left. TA, truncus arteriosus; VE, ventricle. Scale bars, 50 μm.

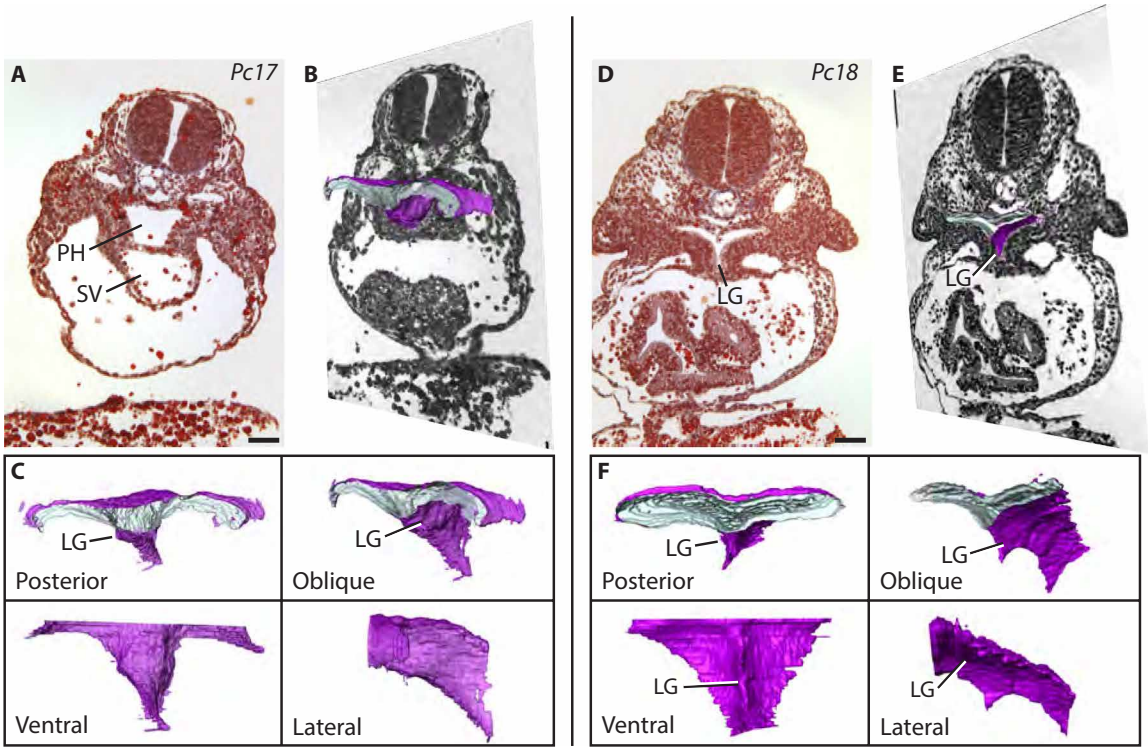

Fig. 4. Formation of the LG in the lungless salamander *P. cinereus* visualized by using μCT. (**A** to **C**) Pharyngeal and foregut morphology at stage *Pc17*: (A) Transverse histological section through the putative lung region shows a wide, rectangular pharynx (PH) dorsal to the sinus venosus (SV). (B) Oblique lateral view of a 3D reconstruction of an endocast of the pharynx (purple) overlaid on a representative orthoslice. (C) Pharyngeal endocast viewed from posterior, oblique lateral, ventral, and lateral perspectives; interior lumen is shaded gray. The LG is beginning to form. (**D** to **F**) Stage *Pc18*: (D) Transverse histological section; the LG is well developed. (E) Oblique lateral view of a three-dimensional (3D) reconstruction of an endocast of the pharynx (purple) overlaid on a representative orthoslice. (F) The pharyngeal endocast viewed from posterior, oblique lateral, ventral, and lateral perspectives. Scale bar, 100 μm.

that of lunged *A. mexicanum*. Signs of regression, first visible during late-stage *Pc21*, include shortening and collapse of the tube (Fig. 5E). Rates of apoptosis in the lung rudiment were assessed by terminal deoxynucleotidyl transferase–mediated deoxyuridine triphosphate nick end labeling (TUNEL) at stage *Pc20*, before morphological indications of regression, and compared to rates in *A. mexicanum* at a similar stage (*Am41*; Fig. 6A). Rates are significantly higher in *P. cinereus* ($P < 0.05$; 6.3 ± 0.64%, $N = 4$ versus 1.2 ± 0.14%, $N = 4$; Fig. 6C). Apoptotic figures are found mainly in the proximal LT and the surrounding anteroventral mesenchyme (Fig. 6B). No apoptosis is visible in the mesenchyme surrounding the caudal tip of the LT, and very few apoptotic cells are seen throughout the rest of the embryo. The lung rudiment continues to morphologically regress during stage *Pc22*, when there is no longer any sign of an epithelial evagination and a long, thin strip of mesenchymal cells occupies the former location of the LT (Fig. 5F). By stage *Pc23*, there is no sign of either the condensed mesenchyme or the epithelial diverticulum (Fig. 5, G and H).

A lung rudiment also forms in embryos of the plethodontid species *H. scutatum* and *D. fuscus* (Fig. 7). LT development and regression in *D. fuscus* closely resembles that of *P. cinereus*, whereas in *H. scutatum* the rudiment appears to be present for a shorter duration. In all plethodontid species examined, the LT emerges at the embryonic stage when the gills begin to branch and in the same axial position as the LT in *A. mexicanum*—dorsal to the division between the atrium and sinus venosus of the heart.

Genetic markers of lung development are expressed in plethodontid salamanders

In embryos of *P. cinereus*, *Wnt2b*, a marker of lung specification, is expressed at stage *Pc18* in two mesenchymal domains that surround the LG (Fig. 8A), precisely matching the pattern observed in other vertebrates, including *Xenopus laevis* (*28*) and mammals (*23*, *33*). Expression persists during formation of the LT at stage *Pc19* (Fig. 8, B and C), when the lung rudiment begins to express *Nkx2.1*, an early marker of pulmonary identity, specifically along its luminal surface (Fig. 8, D to F). This latter expression persists until *Pc21*, when the rudiment begins to regress. *Sox9*, a marker for pulmonary differentiation and distal lung identity, is expressed broadly at stage *Pc19*, including in the lung rudiment, but its expression is stronger and more specific to the LT at stage *Pc21* (Fig. 8, G and H). *Sox9* expression is also observed in the head and heart. In *A. mexicanum*, *Sox9* is weakly expressed in the lungs at stage *Am42*, but expression intensifies in the luminal surface of the lung by stage *Am44*.

Several genetic markers of developing and mature mammalian lungs have been identified through bioinformatic and genetic methods (*34*, *35*), and expression patterns of many of them are conserved in lunged amphibians [e.g., *Xenopus*; (*28*)]. We sequenced the transcriptome of the LT of *P. cinereus* at stages *Pc19* and *Pc21* to determine whether the gene expression profile of the LT overlaps with that of a developing lung. LT transcriptomes for embryonic *A. mexicanum* (stage *Am40*) and a single juvenile lung sample were compared to *P. cinereus* LT transcriptomes to assess lung marker

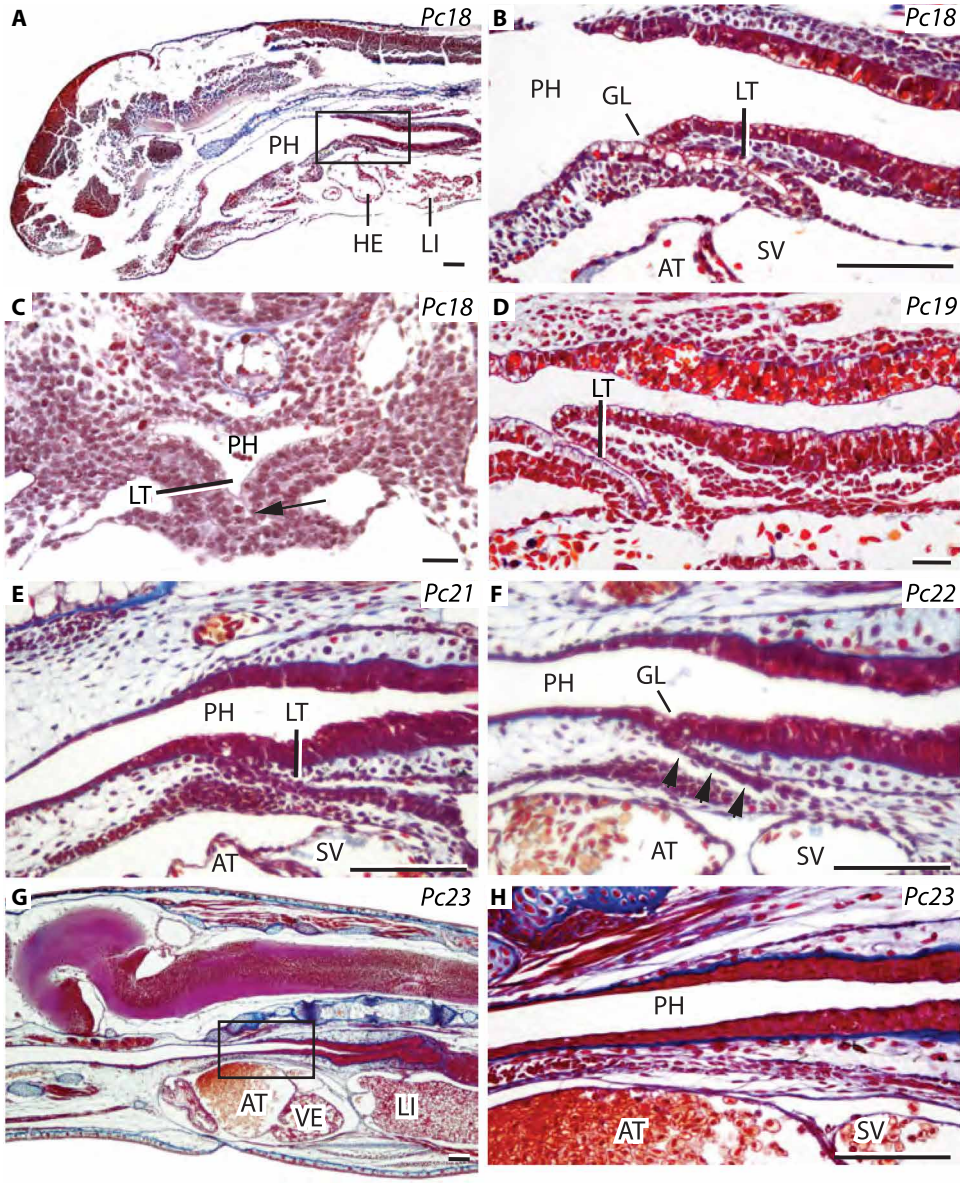

Fig. 5. Embryonic formation and regression of the LT in the lungless salamander *P. cinereus*. (**A** and **B**) Distinct glottis (GL) and LT form at stage *Pc18*. Boxed area in (A) is enlarged in (B). (**C**) Initially, the LT diverticulum is flattened ventrally and bears slight lateral flanges (arrow), which precede formation of paired lung buds. (**D**) By stage Pc19, the LT has elongated ventrally and caudally; its lumen is lined by a simple cuboidal epithelium surrounded by ventral mesenchyme. (**E** and **F**) Later sections show incremental collapse of the LT during stages *Pc21* and *Pc22*, when it forms a band of thin mesenchyme with only a small endodermal outpocketing (arrowheads). (**G** and **H**) The LT is absent by stage *Pc23*, before hatching. Boxed region in (G) is enlarged in (H). (A), (B), and (D) to (H) are midsagittal sections; anterior is to the left; (C) is a transverse section. LI, liver. Scale bars, 50 μm (B to E and H) and 150 μm (A and G).

expression (Table 1). *P. cinereus* expresses a number of markers for alveolar type II cells in the LT, including *Lamp3*, *Abca3*, and all four pulmonary surfactant proteins A, B, C, and D. Markers of proximal or distal lung identity, such as *Sox2*, *FoxJ1*, and the aforementioned *Sox9*, are also expressed at both developmental stages, as are lung development markers such as the *Fgf10*-induced transcription factors *Etv4* and *Etv5*. These expression data offer further evidence that lungs begin to form in lungless salamanders and of the homology of the LT from *P. cinereus* to the LT from *A. mexicanum* and other lunged tetrapods.

Differential expression analysis comparing two embryonic stages of *P. cinereus* reveals both up-regulation and especially down-regulation of several genes (tables S1 and S2). The *Wnt* effector β-catenin (*Ctnnb1*) is significantly down-regulated at *Pc21* relative to *Pc19*, as are the apoptotic regulators *Bcl2l1*; the latter decrease is a signature of apoptosis. At the same time, *Fgf2*, which induces *Nkx2.1* early in lung development and later has a role in alveolar differentiation (*36*, *37*), is up-regulated between *Pc19* and *Pc21*. Gene ontology (GO) term enrichment analysis was used to examine broad categories of differentially regulated genes. Several GO categories related

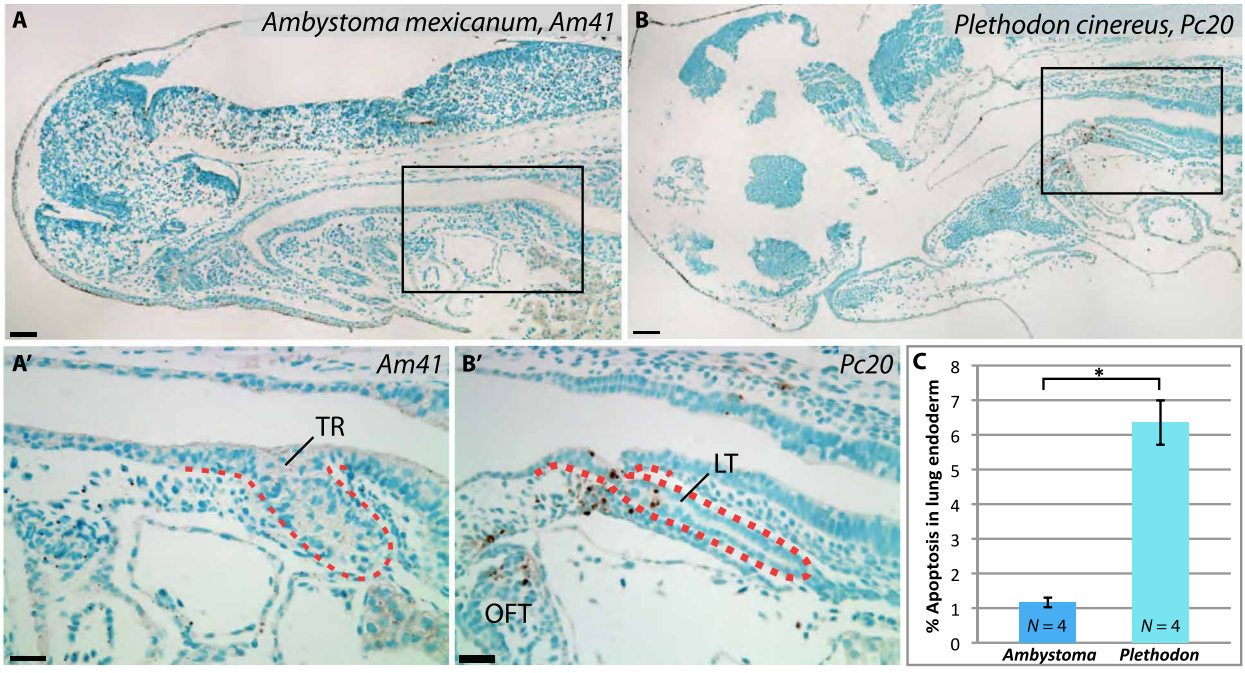

Fig. 6. The lung rudiment in plethodontid embryos regresses by apoptosis. (**A** and **A'**) Embryos of *A. mexicanum* at stage *Am41* display few apoptotic cells in the foregut region as assessed by TUNEL staining. The red dashed line outlines the trachea (TR). Boxed area in (A) is enlarged in (A'). (**B** and **B'**) Embryos of *P. cinereus* at early-stage *Pc20*, one stage before regression is visible histologically, have numerous apoptotic cells (brown staining) in the LT and surrounding mesenchyme. Few apoptotic cells are present in other tissues. Boxed area in (B) is enlarged in (B'). OFT, outflow tract (heart). (**C**) The rate of apoptosis in endoderm of the lung rudiment is significantly higher in *P. cinereus* (Mann-Whitney *U* test, $P < 0.05$). Vertical brackets indicate one SE on either side of each mean value. (A) and (B) depict midsagittal sections; anterior is to the left. Scale bars, 100 μm (A and B) and 50 μm (A' and B').

to apoptosis are overrepresented in the genes up-regulated at *Pc21*, presaging the regression of the lung rudiment (fig. S1). These categories include B cell apoptotic process and its regulation, lymphocyte apoptotic process and its regulation, and leukocyte apoptotic process.

Lunged-salamander mesenchyme promotes pulmonary diverticulum development in lungless salamanders

Reciprocal signaling between foregut endoderm and underlying mesoderm mediates lung specification and morphogenesis (*38*). We attempted to prolong lung development in embryos of the lungless species *H. scutatum* by heterospecific transplantation of splanchnic mesoderm from embryonic *A. mexicanum*. These experiments assess the extent to which arrested development of the pulmonary rudiment in lungless salamanders may be due to the absence of appropriate inductive signals from mesoderm as opposed to diminished competence of the foregut endoderm.

Homotypic donor grafts of green fluorescent protein–positive (GFP^+) *A. mexicanum* lateral plate mesoderm (LPM) were transplanted into *H. scutatum* host embryos at the 3- or 4-somite stage, and the resulting chimeras were reared for approximately 30 days (Fig. 9). Of 80 unilateral transplantations attempted, 49 survived. Of these, nine (18%) show advanced pulmonary development. In each case, an ectopic endodermal diverticulum emerges from foregut endoderm dorsal to the heart and is surrounded by GFP^+ splanchnic mesoderm derived from *A. mexicanum* (Fig. 9, C and D). The unicameral diverticulum extends caudally, ventral to the liver, and appears light-colored in whole mounts (Fig. 9C). This tube is always unpaired, perhaps reflecting the exclusively unilateral grafts. Six of the surviving chimeras were sectioned and immunostained for GFP. In each one, a clearly visible ectopic endodermal diverticulum composed of a spongy, columnar epithelium is invested by *A. mexicanum*–derived splanchnic mesoderm (Fig. 9, G and H). One chimera even has a glottis-like structure proximally with underlying donor-derived mesenchyme (Fig. 9F). None of the mock transplant controls, in which the ectoderm was peeled back from *H. scutatum* embryos, then the LPM was first excised and then transplanted back in place, developed lung-like structures. Transplant recipients were not examined for molecular markers of lung development due to the absence of in situ probes for *H. scutatum* and the lack of cross-reactive antibodies for pulmonary endoderm in salamanders.

DISCUSSION

Lung development in lungless salamanders

Lungless salamanders (Plethodontidae) are not lungless, or at least not as embryos. Instead, plethodontid embryos begin to form lungs, which regress before hatching. Initial development of the lungs in plethodontid salamanders and in *A. mexicanum* (Ambystomatidae) coincides with the onset of gill branching. Similarly, a transient LT arises at precisely the same axial location in both plethodontids and *A. mexicanum*, viz., dorsal to the division between the atria and the sinus venosus of the heart (Figs. 1B,2 to 5, and 7). This morphological structure is present in embryos of *P. cinereus*, *D. fuscus*, and *H. scutatum*. These three species together constitute a broad phylogenetic sampling of plethodontid salamanders, representing both of the currently recognized subfamilies, Plethodontinae and

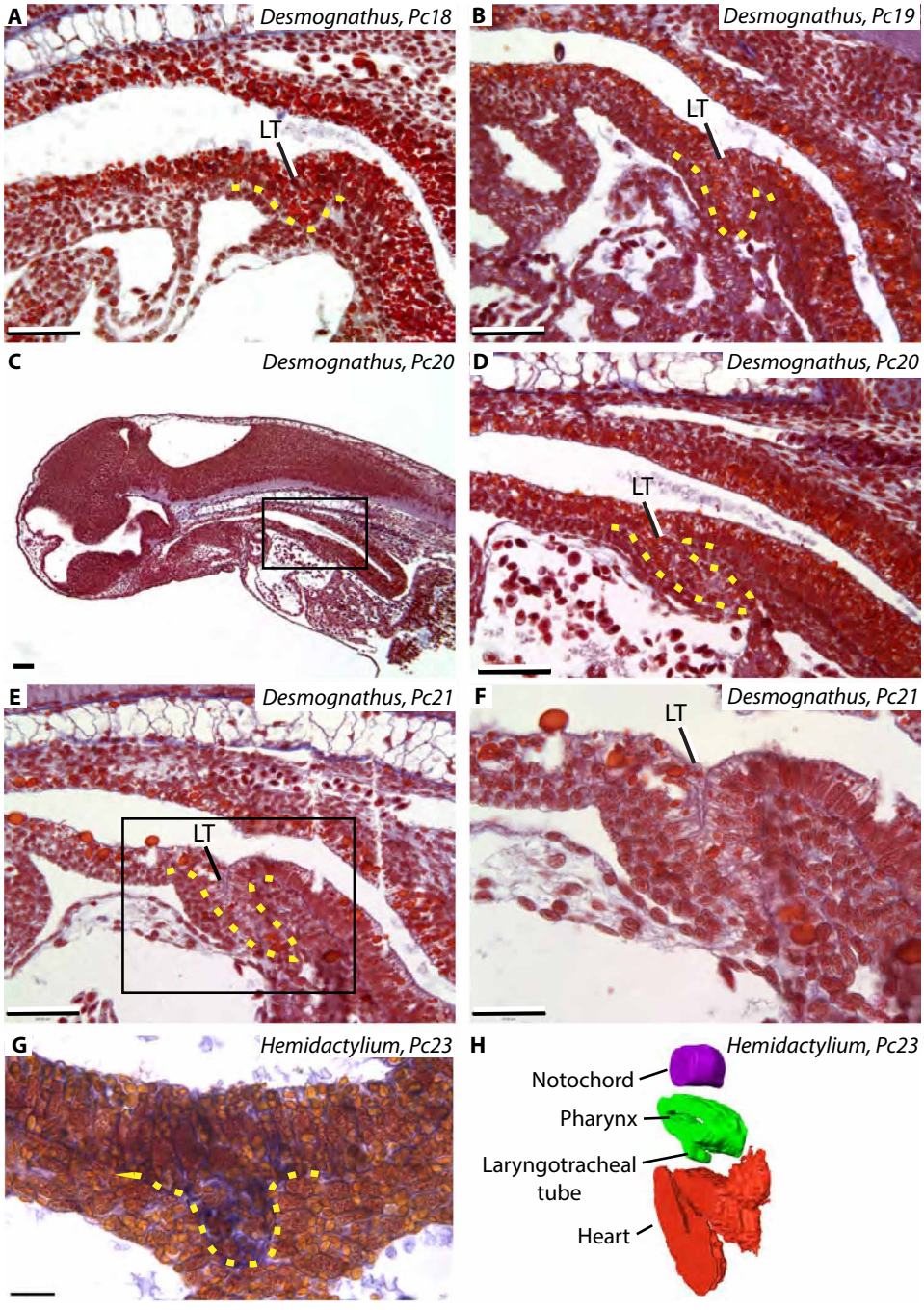

Fig. 7. An LT also forms in the lungless salamanders *D. fuscus* and *H. scutatum*. (**A**) The LT forms at stage *Pc18*. Its endodermal extent is outlined by a yellow dashed line. (**B** to **D**) The LT diverticulum elongates during stages *Pc19* and *Pc20*. Boxed area in (C) is enlarged in (D). (**E** and **F**) The LT appears to collapse distally and stop elongating at stage *Pc21*. Boxed area in (E) is enlarged in (F). (**G**) Transverse section through the LT. (**H**) 3D histological reconstruction of the LT from (G) in an oblique lateral view. (A) to (F) are midsagittal sections; anterior is to the left. Scale bars, 100 μm (A to E and H) and 50 μm (F and G). Stages are matched to those of *P. cinereus* (*68*); for *Hemidactylium*, *Pc23* is roughly equivalent to *Hs28* (*69*).

Hemidactyliinae (*22*, *39*), and two different life histories. We see no indication, however, that life history mode is correlated in any pronounced way with development of the lung rudiment, including its duration. For example, development and regression of the LT in *D. fuscus*, a metamorphosing species, closely resembles that in *P. cinereus*, a direct developer, whereas the rudiment is present for a shorter duration in *H. scutatum*, another metamorphosing species. In *P. cinereus*, the lung rudiment expresses several genetic markers typically associated with pulmonary development in lunged vertebrates (Fig. 8). Expression of *Wnt2b* in mesenchyme flanking the LG, the precursor to the LT, is identical to expression that mediates lung specification in frogs (*28*) and mice (*23*). Once the LT forms, it

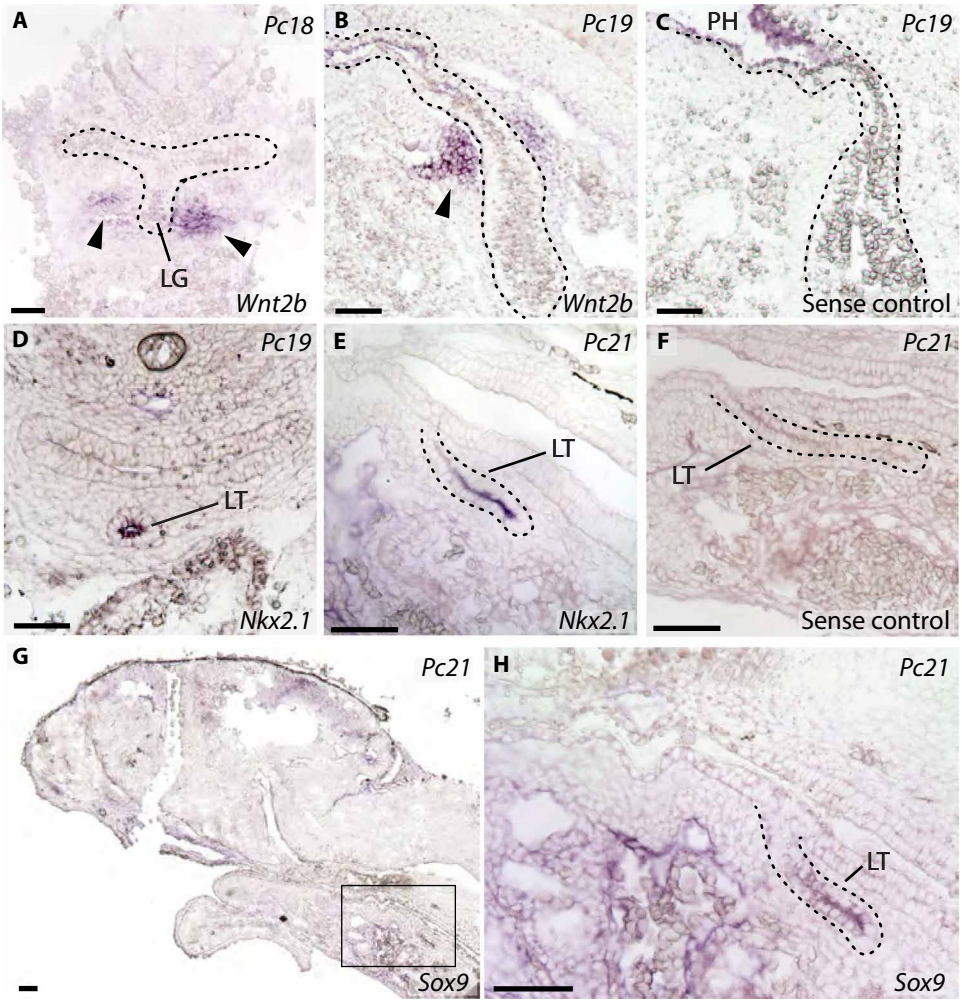

Fig. 8. Embryos of *P. cinereus* express markers of lung specification and development. (**A** to **C**) *Wnt2b* is expressed before and during outgrowth of the LT. Dashed lines outline the pharynx and foregut. (A) The LG is flanked by lateral foci of *Wnt2b*-expressing mesenchyme (arrowheads) in a transverse section at stage *Pc18*. (B) *Wnt2b* is expressed lateral to the LT in a parasagittal section at stage *Pc19*. Anterior is to the left. (C) Negative control with labeled *Wnt2b* sense-strand probe of a section at the same position as (B). While some probe-trapping is visible in the pharynx (PH), adjacent mesenchyme is unstained. (**D** to **F**) *Nkx2.1* is expressed in the LT. (D) Transverse section at stage *Pc19*. (E) *Nkx2.1* is expressed specifically in luminal cells that line the LT (dashed line). Midsagittal section; anterior is to the left. (F) Negative control with labeled *Nkx2.1* sense-strand probe. (**G**) *Sox9* is expressed in the LT at stage *Pc21*. Midsagittal section; anterior is to the left. (**H**) Boxed area in (G). *Sox9* is expressed throughout most of the LT (dashed line). Scale bars, 100 μm.

expresses the homeobox gene *Nkx2.1*, the earliest specific marker of pulmonary identity (*26*–*28*, *40*), and by stage *Pc21*, the LT expresses the distal pulmonary marker *Sox9* (*28*, *29*).

In *P. cinereus*, the lung rudiment continues to develop for approximately 3 weeks (at a rearing temperature of 15°C) before it begins to regress. Regression occurs by apoptosis, particularly in the proximal epithelium (Fig. 6). Since a rudiment is specified and then develops for a substantial period, lung regression may represent the cessation of lung growth and/or the loss of lung maintenance. Alternatively, cues for active degeneration may cause developmental arrest and regression.

Lung rudiment specification and morphogenesis, and the expression of pulmonary markers, illustrate that portions of the ancestral vertebrate lung-development pathway have been conserved in plethodontids over the millions of years of evolutionary history since lungs were lost in adults. Pleiotropy offers one possible explanation. The lung rudiment, for example, may play important roles in the development of adjacent organs such as the heart (*7*, *33*, *41*–*44*), or the gene-regulatory networks that govern initial lung formation are conserved because of their pleiotropic roles in the development of other organs, such as the gene Sonic hedgehog (*Shh*) in limb development (*3*, *45*, *46*). A similar phenomenon is seen in the living coelacanth, *Latimeria chalumnae*, in which a well-developed and potentially functional lung forms in the embryo but is reduced to a vestigial, nonfunctional lung in the adult (*1*). This vestige, however, is closely associated with a unique buoyancy organ, the "fatty organ," whose initial development may require the presence of a lung.

Observed patterns of gene expression also provide insights into the developmental mechanism that mediated evolutionary lung loss. *Sox9*, for example, plays a role in tracheal cartilage development and distal lung morphogenesis (*34*, *47*). In embryonic mice, the gene is

Table 1. Lung marker expression in embryonic lung rudiments of lungless *P. cinereus* and in embryonic and juvenile lungs of *A. mexicanum*. Black squares indicate genes that were identified by tblastn or blastp searches. *E* values represent blast hits between *P. cinereus* and the noted annotated gene. Transcripts *Nkx2.1* through *Etv5* are expressed in embryonic cells before cell type differentiation. AT2, alveolar type 2; Cpict, *Chrysemys picta bellii*; Fdama, *Fukomys damarensis*; Ggall, *Gallus gallus*; Hsap, *Homo sapiens*; Xlaev, *Xenopus laevis*; Xtrop, *Xenopus tropicalis*.

Gene	*P. cinereus*		*A. mexicanum*					
	Stage *Pc19*	Stage *Pc21*	Stage *Am40*	Adult	Cell type	*E* value	NCBI accession	PC ID
Sftpa	■	■	■	■	AT2	1e−55 (Ggall)	NP_989937.1	c1013790_g1_i1
Sftpb	■	■	■	■	AT2	4e−73 (Xlaev)	ABH09132	c367617_g1_i1
Sftpc	■		■	■	AT2	4e−17 (Fdama)	XM_010624309.1	c4587_g1_i1
Sftpd	■	■		■	AT2	3e−94 (Cpict)	AEJ87258.1	513945_g2_i1
Lamp3	■	■	■	■	AT2	2e−25 (Xtrop)	XP_002936919.2	c477495_g1_i1
Abca3	■	■	■	■	AT2	5e−109 (Xtrop)	XP_002932496.2	c517315_g2_i1
Napsa	■	■	■	■	AT2	1e−140 (Xtrop)	NP_001005701.1	c509674_g3_i1
Ctsh	■	■	■	■	AT2	1e−58 (Xtrop)	NP_001011295.1	c503069_g1_i1
Sox2	■	■	■	■	Proximal	4e−66 (Xtrop)	NP_998869.1	c461800_g1_i4
Sox9	■	■	■	■	Distal	6e−125 (Xtrop)	NP_001016853.1	c491172_g2_i1
Foxj1	■	■	■	■	Ciliated	2e−45 (Xtrop)	Q5M7N6.2	c597436_g1_i1
Nkx2.1	■		■	■		4e−27 (Xtrop)	XP_002935383.1	c830881_g1_i1
Gata6	■	■	■	■		2e−92 (Xlaev)	NP_001083725.1	c462591_g2_i1
Foxa2	■	■	■	■		1e−91 (Xtrop)	Q7T1R4.1	c478790_g5_i1
Wnt2b	■	■	■	■		3e−86 (Xtrop)	EF447424.1	c107573_g1_i1
Chia		■	■			3e−91 (Hsap)	NP_970615.2	c364012_g1_i1
Wnt7b	■	■	■	■		3e−121 (Xlaev)	AAI69513.1	c744606_g1_i1
Etv4	■	■	■			5e−167 (Xlaev)	NP_001083817.1	c475887_g1_i1
Etv5	■	■	■			9e−121 (Hsap)	CAG33048.1	c475887_g1_i1

expressed in lung mesenchyme surrounding the trachea and in distal lung epithelium (*29*). Its expression in LT epithelium of *P. cinereus* suggests a distal identity of the LT in plethodontids. Mutations often act modularly to promote proximal (tracheal) or distal (lung) development ventrally or esophageal development dorsally (table S3) (*48*). Examples include knockouts of the genes *Shh* and *Bmp4*, which specifically abrogate tracheal development while partial lungs still form (*49*, *50*). Both *Shh* and *Bmp4* knockout phenotypes are likely mediated through down-regulation of *Nkx2.1* (*51*), and they contrast with *Fgf10* knockout models, in which the trachea develops but distal lung development is mostly inhibited (*52*). Expression of *Sox9* throughout the LT (Fig. 8) suggests that lungless salamanders lack the proximal portion of their lungs and trachea in a manner consistent with mutations that lead to decreased *Nkx2.1* expression.

In mammals, most known mutations associated with lung loss or developmental arrest are in signaling molecules (table S3) (*37*). This outsized role of signaling pathways in lung development reflects the dependence of lung patterning on a series of reciprocal interactions between the endoderm and underlying mesoderm (*26*, *38*). The same signaling pathways are conserved across vertebrates, and experimental perturbation of these pathways results in lung loss in frogs (*25*). Transplantation of LPM from a lunged salamander into *H. scutatum*, a lungless species, extends lung development into post-embryonic stages (Fig. 9). In other words, the foregut endoderm of *H. scutatum*, and presumably other plethodontid species, remains competent to respond to pulmonary inductive cues and extend the development of pulmonary diverticula, whereas the splanchnic mesoderm appears not to produce the inductive or maintenance signals required to prolong lung development. Lung loss likely reflects altered expression of signaling molecules that mediate later stages of tracheal and pulmonary development.

Lung primordia transcriptomes for two embryonic stages of *P. cinereus* present an opportunity to investigate the differential expression of transcripts between critical developmental time points and further probe possible mechanisms of lung loss in adult plethodontids. Because of the numerous potential pitfalls and biases associated with controlling for species-specific transcriptional differences (*53*), we did not attempt to analyze cross-species differential expression between *Plethodon* and *Ambystoma*. While in situ hybridization reveals typical canonical *Wnt* signaling during early stages of lung development at *Pc18* and *Pc19* (Fig. 8, A to C), down-regulation of the *Wnt* effector β-catenin (*Ctnnb1*) by *Pc21* suggests that canonical *Wnt* signaling decreases during lung regression. Multiple studies support the strong dependence of lung development on canonical *Wnt* signaling (*23*–*25*, *54*), but the role of *Wnt* varies with time. Early signaling is involved in lung specification (*25*), whereas later signaling serves primarily to promote distal alveolar epithelial identity (*55*) and overactivation of *Wnt* signaling at later stages inhibits lung differentiation (*56*). Differential expression of *Ctnnb1* between *Pc19* and *Pc21* may be indicative of defective lung differentiation in *P. cinereus*.

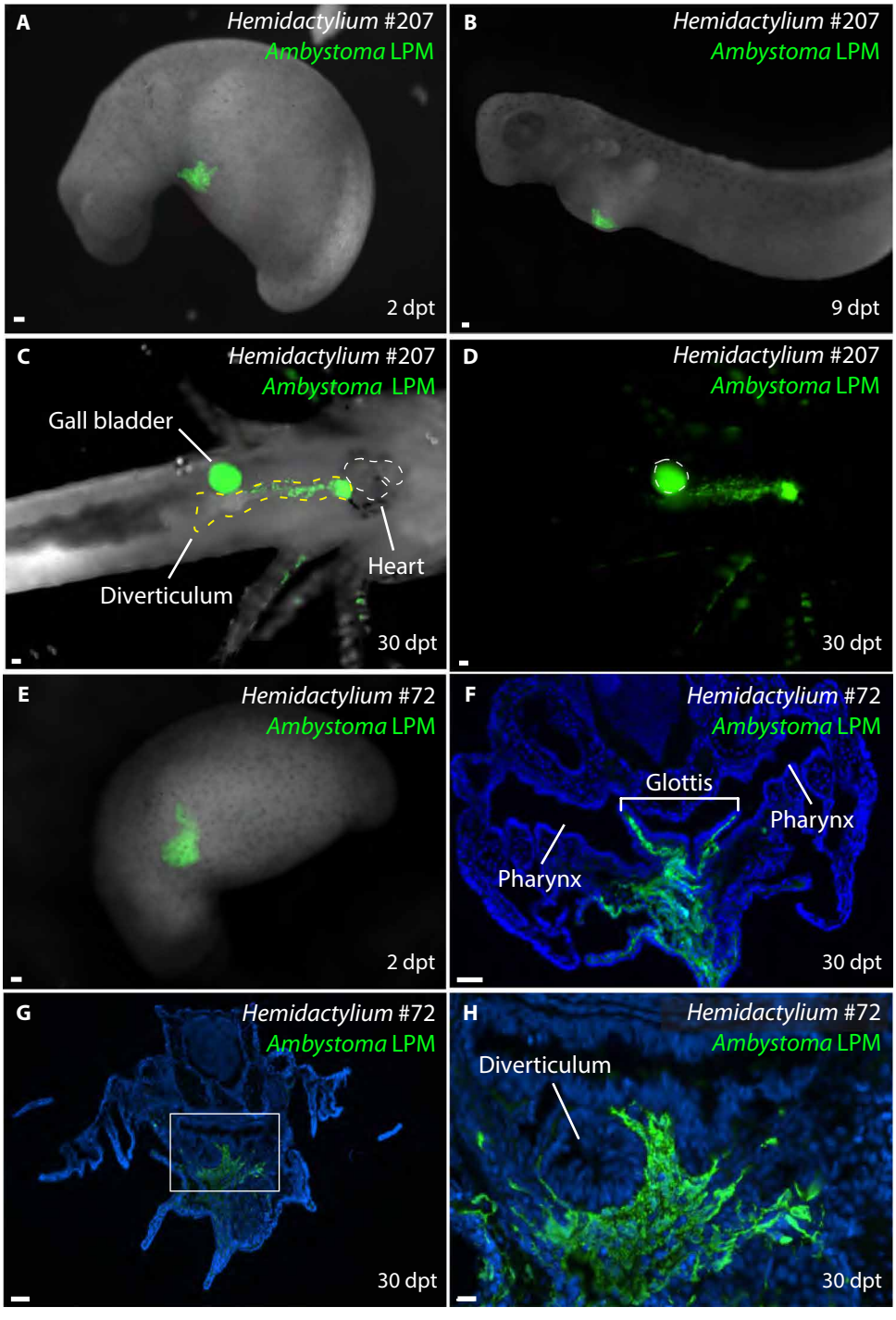

Fig. 9. Transplantation of lunged *A. mexicanum* lateral plate mesoderm (LPM) into lungless *H. scutatum* generates a putative lung. (**A** to **D**) Same transplant recipient 2, 9, and 30 days posttransplant (dpt). The *A. mexicanum* graft is GFP$^+$ and has contributed to splanchnic mesoderm surrounding the foregut. (A and B) Lateral views; anterior is to the left. (C and D) Ventral views of the larva at 30 dpt, with and without bright-field illumination, illustrate formation of an ectopic median diverticulum surrounded by *A. mexicanum*–derived splanchnic mesoderm (dashed yellow line). The diverticulum emerges from the pharynx dorsal to the heart (dashed white line) and terminates ventral to the liver. The gallbladder emits autofluorescence, as do some pigment cells in the skin. (**E** to **H**) Transplant recipient #72 2 and 30 dpt. (E) Lateral view; anterior is to lower left. (F) Transverse section through the pharynx illustrates formation of a glottis supported by *A. mexicanum*–derived splanchnic mesoderm. (G) A more posterior section shows the ectopic diverticulum, which emerges from the foregut. (H) Enlargement of boxed region in (G). Scale bars, 100 μm (A to G) and 50 μm (H).

Homology of the lung rudiment in plethodontids

Both morphological and, increasingly, genetic data have been used to establish the homology of lungs among distantly related vertebrates and between lungs and other respiratory organs, such as the swim bladder of ray-finned fishes (*1*, *57*). Data presented here offer definitive evidence that lungs begin to form in plethodontid salamanders and of their homology with the lungs of other tetrapods.

The search for a lung rudiment in plethodontid salamanders began soon after lunglessness was discovered in the late 19th century and continued for decades. Both Wilder (*16*) and Lüdike (*15*) claimed to observe a vestigial glottis in adults, although Mekeel (*18*) was unable to document even a rudimentary glottis in her study of *P. cinereus*, *D. fuscus*, and *H. scutatum*. On the basis of our ontogenetic data and examination of adult animals, we believe that both Wilder and Lüdike misidentified as the glottis an unrelated transverse fold in the floor of the pharynx that forms embryonically as the initial primary tongue is replaced by the secondary (soft) tongue [Figs. 1, A and B, and 2A in Budzik *et al.* (*58*)]. Mekeel (*18*), relying solely on developmental morphology, was the first person to report a transient lung rudiment in plethodontids. Our observations largely concord with hers, including the presence early of lateral outpocketings from the pharynx, which in a lunged salamander presage formation of paired lung buds, and the coincidence of initial stages of lung formation with the onset of gill branching, as occurs in lunged salamanders. We do not, however, replicate Mekeel's observation that the caudal portion of the rudimentary lung forms vestigial endodermal tissue in the dorsal wall of the sinus venosus following regression. Aside from a single conference abstract, Mekeel's results never appeared in an academic journal, and we have found only four studies published in the subsequent 90 years that cite either that abstract or her unpublished dissertation (*8*, *59*–*61*). It is very unfortunate that this talented young woman's discovery was not published in full or more broadly publicized, and that she has not received due credit for her important contribution.

We regard the LTs of plethodontid and lunged salamanders to be homologous based on their shared timing of emergence, embryonic morphology, axial position, and expression of several pulmonary-associated candidate genes assessed by in situ hybridization. Transcriptome profiling of the LT further reveals that many additional lung genetic markers are also expressed within this tissue (Table 1). In principle, the LT of plethodontids might be confused with the embryonic ultimobranchial body, which also forms as a transient endodermal diverticulum and ultimately fuses to the thyroid. The ultimobranchial body, however, develops far anterior and lateral to the lung rudiment and is derived from a paired pharyngeal pouch (*31*, *62*–*65*). Neither property applies to the LT.

Both morphological and molecular data corroborate that the lungless salamanders (Plethodontidae) undergo early stages of pulmonary development and form a lung rudiment, which subsequently regresses by apoptosis. Expression in the transient rudiment of several genetic markers of lung specification and differentiation suggests evolutionary conservation of inductive interactions that govern at least initial stages of lung formation in tetrapods generally. It is not possible at present to pinpoint exactly when during the early history of plethodontids lungs were lost from adults. The plethodontid fossil record is sparse, and even if it were rich, it would be difficult to infer the presence or absence of "soft" respiratory structures such as lungs, which typically fossilize poorly (*66*). Recent molecular phylogenetic analysis posits divergence among extant plethodontid clades beginning around 66 Ma ago (*22*). If adult lung loss evolved once in the common ancestor of all living species, then in theory this might have occurred anytime between 66 and 110 Ma ago, when Plethodontidae diverged from Amphiumidae, its closest living—and lunged—relative. Alternatively, it is possible that lung loss instead evolved independently in different plethodontid lineages subsequent to their initial diversification. The oldest fossil plethodontids, from the late Oligocene around 25 Ma ago, are assigned to living genera *Aneides* and *Plethodon* (*22*, *67*); these records likely set a minimum age for the evolution of lunglessness in the clade. Regardless of the exact timing of lung loss in plethodontids, studying its developmental basis provides insights into the mechanisms that underlie macroevolutionary organ loss associated with a major evolutionary radiation. This, in turn, opens future avenues to explore the genetic basis of plethodontid lung loss in greater detail and to determine whether lung loss in other vertebrate lineages has evolved by similar or different means.

MATERIALS AND METHODS

Experimental design

The study sought (i) to assess the presence or absence of a lung rudiment in plethodontid salamander embryos based on both morphological and genetic criteria; (ii) following discovery of a lung rudiment, to establish whether the mechanism underlying its regression and loss before hatching involves programmed cell death (apoptosis); (iii) to identify whether the rudiment retains key genetic signaling components characteristic of lung development in vertebrates generally; and (iv) to begin to assess experimentally whether the plethodontid lung rudiment is capable of sustaining lung development to later stages when exposed to appropriate cues from lunged-salamander precursors. Analytical and experimental methods include standard histology, micro–computed tomography (μCT), in situ gene expression and transcriptome sequencing, quantification of apoptosis via TUNEL staining, and heterospecific transplantation of LPM between lunged and lungless salamander embryos. The Mexican axolotl, *A. mexicanum*, was used as a reference lunged salamander.

Embryo collection and husbandry

Animal protocols were approved by Harvard University's Institutional Animal Care and Use Committee (protocol 99-09). Plethodontid embryos were collected under Massachusetts Division of Fisheries and Wildlife (DFW) permits and, where needed, additional local permits: DFW 181.10SCRA (2010), 080.11SCRA (2011), 080.11SCRA (2012), 027.13SCRA (2013), 083.14SCRA (2014), and 022.15SCRA (2015); Cape Cod National Seashore CACO-00214 (table S4).

Embryos were maintained at 15° to 17°C on filter paper moistened with 0.1× MMR (Marc's Modified Ringer solution: 0.01 M NaCl, 0.2 mM KCl, 0.1 mM $MgSO_4$, 0.2 mM $CaCl_2$, and 0.5 mM Hepes, pH 7.4) and gentamicin (100 μg/ml; Sigma-Aldrich, St. Louis, MO) or fully immersed in that solution. They were monitored daily for fungal infections, which were treated by dechorionating embryos and rearing in solution. Staging was performed as described for *P. cinereus* (*68*) and *H. scutatum* (*69*). *D. fuscus* stages correspond to those in *P. cinereus*. *A. mexicanum* embryos were obtained from the Ambystoma Genetic Stock Center, University of Kentucky. Embryos were reared in 20% Holtfreter solution at 17°C and staged according to Bordzilovskaya and colleagues (*70*). Developmental stages of each species are abbreviated in the text by using the first letters of the Latin binomial followed by the stage number, e.g., "*Am38*" for

stage 38 of *A. mexicanum*. Embryonic morphologies of *A. mexicanum* and *P. cinereus* are distinct, but it is possible to identify comparable stages of development by noting the formation of several relatively invariant features. These include the formation and branching of external gills and development of the heart, eyes, and limbs (*68*, *70*). We performed all interspecific comparisons at equivalent stages based on these criteria.

Histology

Embryos were fixed in neutral-buffered formalin or Bouin fixative and processed for histology and imaging (*7*).

μCT and histological reconstruction

X-ray CT was performed on specimens stained for several days with phosphomolybdic acid (*7*, *71*). Three-dimensional (3D) reconstructions from μCT data were completed in Amira 6.0 (FEI Visualization Sciences Group, Houston, TX). For 3D reconstruction from histological data, color images of serial sections were made with a compound microscope and converted to monochrome format. The latter images were imported into Amira and aligned using the Align Slices module. Virtual endocasts of pharyngeal and foregut spaces were segmented using the segmentation editor.

Polymerase chain reaction and probe design

RNA from several embryonic stages was extracted using TRIzol reagent (Thermo Fisher Scientific, Grand Island, NY) and converted to cDNA with an iScript cDNA Synthesis kit (Bio-Rad, Hercules, CA). Polymerase chain reaction (PCR) amplicons generated with primers (table S5) were cloned into the pcrII-TOPO vector (Invitrogen, Waltham, MA). Clones were sequenced, and in situ hybridization probes were constructed using Ambion MAXIscript SP6/T7 enzymes (Thermo Fisher Scientific) and digoxigenin-labeled uridine triphosphate (UTP) (Roche, Penzberg, Germany). An in situ probe for *A. mexicanum Sox9* (*72*) was provided by N. Fröbisch. The *Sox9* probe for *P. cinereus* was previously used to reveal limb skeletal patterning in that species (*73*).

In situ hybridization

In situ hybridization was performed as previously described (*8*).

Measuring apoptosis

Apoptotic rates were examined at stages *Pc20* in *P. cinereus* and *Am41* in *A. mexicanum*. Standard TUNEL was performed using an in situ apoptosis detection kit (Trevigen #4810-30-K, Gaithersburg, MD). To calculate the percentage of lung rudiment cells undergoing apoptosis, the numbers of apoptotic and normal cells were counted in sections processed using TUNEL. Cells were counted in ImageJ by distinguishing cell nuclei stained with methyl green from 3,3′-diaminobenzidine (DAB)–positive apoptotic cells. Statistical differences were assessed by using a two-tailed Mann-Whitney *U* test. Figures are reported as the mean ± SEM. Apoptosis was only quantified in the endoderm, but *Plethodon* showed a large amount of mesenchymal apoptosis that was not quantified. Endodermal and mesenchymal tissues are easily distinguished on the basis of their physical separation and the epithelial morphology of endoderm.

Transcriptome sequencing

Total RNA was extracted from cryosections of lung rudiments for transcriptome sequencing. For cryopreservation, specimens were anesthetized using tricaine (MS-222, 0.02%, pH 7.4; Sigma-Aldrich) and then immersed for 15 min each in ice-cold 15% sucrose containing tricaine and ice-cold 30% sucrose containing tricaine. Specimens were oriented sagittally and embedded in OCT medium (Sakura Finetek USA, Torrance, CA), frozen in a dry ice/ethanol bath, and stored at −80°C. Each specimen was cryosectioned until an approximately mid-sagittal plane was reached.

Kwik-Fil borosilicate glass capillaries (#M1B150-4; World Precision Instruments, Sarasota, FL) were briefly soaked in DRNAse Free (Argos Technologies, Elgin, IL) and dried. Needles were pulled from these capillaries on a World Precision Instruments PUL1 to the following specifications: external tip diameter, ca. 0.14 mm; external diameter (unpulled region), ca. 1.15 mm; sidewall thickness (unpulled region), ca. 0.26 mm; internal diameter (unpulled region), ca. 0.62 mm; length of tapered region, ca. 3.6 mm.

Sectioned specimens, still affixed to an aluminum chuck, were mounted in dry ice and placed under a dissecting microscope. The lung bud region was dissected out by plunging the tip of the glass needle into the tissue just dorsal to the wall between the sinus venosus and the atrium. Endoderm and mesoderm were not separated. Three biological replicates each were obtained for two stages, *Pc19* and *Pc21*. Tissue was expelled or placed into an Eppendorf tube containing lysis buffer and tris(2-carboxyethyl)phosphine (TCEP) from a NucleoSpin RNA XS kit (#740902.10; Machery-Nagel, Düren, Germany). Total RNA was isolated according to the kit protocol, but carrier RNA was not used.

Transcriptome libraries were prepared and sequenced as previously described (*8*). An initial 2 × 150–base pair (bp) Illumina HiSeq 2500 Rapid Run lane was used to assess clustering and relative concentrations (Illumina Inc., San Diego, CA). A second lane was run with adjustments based on the first sequenced flow cell to optimize clustering. This second lane yielded 184.5 million reads that passed filter for a total of 232.4 million reads.

Reads were trimmed with Trimmomatic (*74*). Reads from multiple flow cells were concatenated; reads from multiple libraries within each species were concatenated before de novo assembly. Ribosomal RNA (rRNA) reads were removed using Bowtie (*75*) using a database of deposited rRNA sequences from National Center for Biotechnology Information (NCBI) GenBank. Trinity (release r20140413) was used for de novo assembly, setting --min_kmer_cov to 2 (*76*, *77*). The Trinity assembly was translated using Transdecoder (*76*). Initial annotation was performed using BLASTX and then BLASTP against the Swiss-Prot database. Genes associated with pulmonary identity and lung development were identified by BLAST searches. *E* values are listed in Table 1.

Filtered reads were mapped initially by using RNA-Seq by Expectation-Maximization (RSEM) implemented with the Trinity wrapper. Assemblies were filtered to transcripts that were expressed over 1 fragment per kilobase of exon per million mapped fragments (FPKM) using Trinity, and then reads were remapped to the assembly. Differential expression was analyzed using DESeq normalization (tables S6 to S8) (*78*). GO analysis was performed by annotating each gene with its predicted peptide sequence and importing them into Blast2GO (*79*). Annotations generated with BLASTX (https://blast.ncbi.nlm.nih.gov/) and InterPro (www.ebi.ac.uk/interpro/) were also loaded. Enrichment analysis using Fisher's exact test was used to reveal GO categories over- or underrepresented across experimental conditions.

Heterospecific transplantation

Stage-matched embryos of *H. scutatum* and of ubiquitously expressing GFP^+ *A. mexicanum* at the 3- or 4-somite stage (*Hs18* and *Am19*,

respectively) were placed alongside each other on an agarose plate in 100% Holtfreter solution. LPM from *A. mexicanum* embryos was removed by peeling back the ectoderm using freshly sharpened tungsten needles and then making a rectangular incision through the lateral plate. A comparable piece of lateral plate was excised from *H. scutatum* and replaced with *A. mexicanum* lateral plate. Embryos were allowed to heal for approximately 60 min and then transferred to individual wells of a 12-well dish and maintained in 20% Holtfreter solution plus gentamicin (100 µg/ml). Mock transplants (i.e., negative controls) were performed in parallel: The ectoderm was peeled back from *H. scutatum* embryos, and then the LPM was excised and transplanted back in place. Photographs were taken 1 to 2 days after transplantation and then at fixation at *Hs28* or later (30 days after transplantation). Individuals were cryosectioned at 14- to 16-µm thickness and processed for immunohistochemistry (*80*). Briefly, sections were blocked and then incubated with an anti-GFP primary antibody (#ab290; Abcam, Cambridge, MA), followed by labeling with Alexa Fluor 488 secondary antibody (#Z25302; Thermo Fisher Scientific) and nuclear staining with 4′,6-diamidino-2-phenylindole (DAPI) (Sigma-Aldrich). Failure to obtain a reliable antibody against pulmonary markers prevented molecular colocalization, but graft recipients were assayed for morphology of the foregut region. *H. scutatum* was selected for transplantation because it was possible to obtain large numbers of field-collected embryos, and the mesolecithal eggs closely resemble those of *A. mexicanum*, in contrast to the telolecithal eggs of direct-developing *P. cinereus* (*69*).

Statistical analysis

A Mann-Whitney *U* test was used to compare rates of apoptosis in lung rudiment endoderm between embryos of *A. mexicanum* (stage *Am41*) and *P. cinereus* (stage *Pc20*). The histogram depicts the mean ± SE of the frequency of apoptotic cells in four embryos of each species (Fig. 6C). The analysis was performed by using Microsoft Excel for Mar, v. 16.57; statistical significance was evaluated at $P < 0.05$.

SUPPLEMENTARY MATERIALS

Supplementary material for this article is available at https://science.org/doi/10.1126/sciadv.abo6108

View/request a protocol for this paper from *Bio-protocol*.

REFERENCES AND NOTES

1. C. Cupello, P. M. Brito, M. Herbin, F. J. Meunier, P. Janvier, H. Dutel, G. Clément, Allometric growth in the extant coelacanth lung during ontogenetic development. *Nat. Commun.* **6**, 8222 (2015).
2. B. K. Hall, Developmental mechanisms underlying the formation of atavisms. *Biol. Rev.* **59**, 89–122 (1984).
3. F. Leal, M. J. Cohn, Loss and re-emergence of legs in snakes by modular evolution of sonic hedgehog and HOXD enhancers. *Curr. Biol.* **26**, 2966–2973 (2016).
4. C. Darwin, *On the Origin of Species by Means of Natural Selection, or the Preservation of Favoured Races in the Struggle for Life* (John Murray, ed. 1, 1859).
5. L. Bejder, B. K. Hall, Limbs in whales and limblessness in other vertebrates: Mechanisms of evolutionary and developmental transformation and loss. *Evol. Dev.* **4**, 445–458 (2002).
6. AmphibiaWeb (University of California, Berkeley, 2022); https://amphibiaweb.org.
7. Z. R. Lewis, J. Hanken, Convergent evolutionary reduction of atrial septation in lungless salamanders. *J. Anat.* **230**, 16–29 (2017).
8. Z. R. Lewis, J. A. Dorantes, J. Hanken, Expression of a novel surfactant protein gene is associated with sites of extrapulmonary respiration in a lungless salamander. *Proc. R. Soc. Lond. B Biol. Sci.* **285**, 20181589 (2018).
9. D. Bickford, D. Iskandar, A. Barlian, A lungless frog discovered on Borneo. *Curr. Biol.* **18**, 374–375 (2008).
10. R. A. Nussbaum, M. Wilkinson, A new genus of lungless tetrapod: A radically divergent caecilian (Amphibia: Gymnophiona). *Proc. R. Soc. Lond. B Biol. Sci.* **261**, 331–335 (1995).
11. B. J. van Soldt, B. D. Metscher, R. E. Poelmann, B. Vervust, F. J. Vonk, G. B. Müller, M. K. Richardson, Heterochrony and early left-right asymmetry in the development of the cardiorespiratory system of snakes. *PLOS ONE* **10**, e116416 (2015).
12. N. L. Reagan, P. A. Verrell, The evolution of plethodontid salamanders: Did terrestrial mating facilitate lunglessness? *Am. Nat.* **138**, 1307–1313 (1991).
13. J. A. Ruben, N. L. Reagan, P. A. Verrell, A. J. Boucot, Plethodontid salamander origins: A response to Beachy and Bruce. *Am. Nat.* **142**, 1038–1051 (1993).
14. Z. R. Lewis, "Causes and consequences of lung loss in salamanders," thesis, Harvard University, Cambridge, MA (2016).
15. R. Lüdike, Über den Respirationsapparat verschiedener Urodelen und seine Beziehungen zum Herzen. *Z. Morphol. Ökol. Tiere* **43**, 578–615 (1955).
16. H. H. Wilder, Lungless salamanders. *Anat. Anz.* **12**, 182–192 (1896).
17. A. G. Mekeel, "Pulmonary development in the lungless salamanders," thesis, Cornell University, Ithaca, NY (1930).
18. A. G. Mekeel, A pulmonary vestige in the lungless salamanders. *Anat. Rec.* **34**, 141 (1926).
19. T. Demircan, A. E. İlhan, N. Aytürk, B. Yıldırım, G. Öztürk, İ. Keskin, A histological atlas of the tissues and organs of neotenic and metamorphosed axolotl. *Acta Histochem.* **118**, 746–759 (2016).
20. T. B. Jensen, P. Giunta, N. G. Schultz, J. M. Griffiths, T. J. Duerr, Y. Kyeremateng, H. Wong, A. Adesina, J. R. Monaghan, Lung injury in axolotl salamanders induces an organ-wide proliferation response. *Dev. Dyn.* **2021**, 866–879 (2021).
21. L. D. Miller, S. E. Wert, J. A. Whitsett, Surfactant proteins and cell markers in the respiratory epithelium of the amphibian, *Ambystoma mexicanum*. *Comp. Biochem. Physiol. A Mol. Integr. Physiol.* **129**, 141–149 (2001).
22. X. X. Shen, D. Liang, M. Y. Chen, R. L. Mao, D. B. Wake, P. Zhang, Enlarged multilocus data set provides surprisingly younger time of origin for the Plethodontidae, the largest family of salamanders. *Syst. Biol.* **65**, 66–81 (2016).
23. A. M. Goss, Y. Tian, T. Tsukiyama, E. D. Cohen, D. Zhou, M. M. Lu, T. P. Yamaguchi, E. E. Morrisey, Wnt2/2b and β-catenin signaling are necessary and sufficient to specify lung progenitors in the foregut. *Dev. Cell* **17**, 290–298 (2009).
24. K. S. Harris-Johnson, E. T. Domyan, C. M. Vezina, X. Sun, ß-catenin promotes respiratory progenitor identity in mouse foregut. *Proc. Natl. Acad. Sci. U.S.A.* **106**, 16287–16292 (2009).
25. S. A. Rankin, A. L. Gallas, A. Neto, J. L. Gómez-Skarmeta, A. M. Zorn, Suppression of Bmp4 signaling by the zinc-finger repressors Osr1 and Osr2 is required for Wnt/β-catenin-mediated lung specification in *Xenopus*. *Development* **139**, 3010–3020 (2012).
26. E. A. Hines, X. Sun, Tissue crosstalk in lung development. *J. Cell. Biochem.* **115**, 1469–1477 (2014).
27. P. Minoo, G. Su, H. Drum, P. Bringas, S. Kimura, Defects in tracheoesophageal and lung morphogenesis in *Nkx2.1*(−/−) mouse embryos. *Dev. Biol.* **209**, 60–71 (1999).
28. S. A. Rankin, H. T. Tran, M. Wlizla, P. Mancini, E. T. Shifley, S. D. Bloor, L. Han, K. Vleminckx, S. E. Wert, A. M. Zorn, A molecular atlas of *Xenopus* respiratory system development. *Dev. Dyn.* **244**, 69–85 (2015).
29. A.-K. T. Perl, R. Kist, Z. Shan, G. Scherer, J. A. Whitsett, Normal lung development and function after *Sox9* inactivation in the respiratory epithelium. *Genesis* **41**, 23–32 (2005).
30. J. A. Zepp, M. P. Morley, C. Loebel, M. M. Kremp, F. N. Chaudhry, M. C. Basil, J. P. Leach, C. Liberti, T. K. Niethamer, Y. Ying, S. Jayachandran, A. Babu, S. Zhou, D. B. Frank, J. A. Burdick, E. E. Morrisey, Genomic, epigenomic, and biophysical cues controlling the emergence of the lung alveolus. *Science* **371**, eabc3172 (2021).
31. J. N. Dent, The embryonic development of *Plethodon cinereus* as correlated with the differentiation and functioning of the thyroid gland. *J. Morphol.* **71**, 577–601 (1942).
32. D. B. Wake, J. Hanken, Direct development in the lungless salamanders: What are the consequences for developmental biology, evolution and phylogenesis? *Int. J. Dev. Biol.* **40**, 859–869 (1996).
33. T. Peng, Y. Tian, C. J. Boogerd, M. M. Lu, R. S. Kadzik, K. M. Stewart, S. M. Evans, E. E. Morrisey, Coordination of heart and lung co-development by a multipotent cardiopulmonary progenitor. *Nature* **500**, 589–592 (2013).
34. D. Chang, D. Alanis, R. Miller, H. Ji, H. Akiyama, P. D. McCrea, J. Chen, Lung epithelial branching program antagonizes alveolar differentiation. *Proc. Natl. Acad. Sci. U.S.A.* **110**, 18042–18051 (2013).
35. B. Treutlein, D. G. Brownfield, A. R. Wu, N. F. Neff, G. L. Mantalas, F. H. Espinoza, T. J. Desai, M. A. Krasnow, S. R. Quake, Reconstructing lineage hierarchies of the distal lung epithelium using single-cell RNA-seq. *Nature* **509**, 371–375 (2014).
36. A. E. Serls, S. Doherty, P. Parvatiyar, J. M. Wells, G. H. Deutsch, Different thresholds of fibroblast growth factors pattern the ventral foregut into liver and lung. *Development* **132**, 35–47 (2005).
37. E. E. Morrisey, B. L. M. Hogan, Preparing for the first breath: Genetic and cellular mechanisms in lung development. *Dev. Cell* **18**, 8–23 (2010).
38. D. McCulley, M. Wienhold, X. Sun, The pulmonary mesenchyme directs lung development. *Curr. Opin. Genet. Dev.* **32**, 98–105 (2015).

39. R. A. Pyron, J. J. Wiens, A large-scale phylogeny of Amphibia including over 2800 species, and a revised classification of extant frogs, salamanders, and caecilians. *Mol. Phylogenet. Evol.* **61**, 543–583 (2011).
40. D. Lazzaro, M. Price, M. de Felice, R. Di Lauro, The transcription factor TTF-1 is expressed at the onset of thyroid and lung morphogenesis and in restricted regions of the foetal brain. *Development* **113**, 1093–1104 (1991).
41. B. Devi, J. R. S. More, Total tracheopulmonary agenesis. Associated with asplenia, agenesis of umbilical artery and other anomalies. *Acta Paediatr. Scand.* **55**, 107–116 (1966).
42. M. M. Goddeeris, S. Rho, A. Petiet, C. L. Davenport, G. A. Johnson, E. N. Meyers, J. Klingensmith, Intracardiac septation requires hedgehog-dependent cellular contributions from outside the heart. *Development* **135**, 1887–1895 (2008).
43. A. D. Hoffmann, M. A. Peterson, J. M. Friedland-Little, S. A. Anderson, I. P. Moskowitz, Sonic hedgehog is required in pulmonary endoderm for atrial septation. *Development* **136**, 1761–1770 (2009).
44. L. Xie, A. D. Hoffmann, O. Burnicka-Turek, J. M. Friedland-Little, K. Zhang, I. P. Moskowitz, Tbx5 hedgehog molecular networks are essential in the second heart field for atrial septation. *Dev. Cell* **23**, 280–291 (2012).
45. S. Bellusci, Y. Furuta, M. G. Rush, R. Henderson, G. Winnier, B. L. Hogan, Involvement of Sonic hedgehog (Shh) in mouse embryonic lung growth and morphogenesis. *Development* **124**, 53–63 (1997).
46. R. D. Riddle, R. L. Johnson, E. Laufer, C. Tabin, Sonic hedgehog mediates the polarizing activity of the ZPA. *Cell* **75**, 1401–1416 (1993).
47. G. Turcatel, N. Rubin, D. B. Menke, G. Martin, W. Shi, D. Warburton, Lung mesenchymal expression of *Sox9* plays a critical role in tracheal development. *BMC Biol.* **11**, 117 (2013).
48. E. E. Morrisey, A. K. Rustgi, The lung and esophagus: Developmental and regenerative overlap. *Trends Cell Biol.* **28**, 738–748 (2018).
49. Y. Li, J. Gordon, N. R. Manley, Y. Litingtung, C. Chiang, Bmp4 is required for tracheal formation: A novel mouse model for tracheal agenesis. *Dev. Biol.* **322**, 145–155 (2008).
50. Y. Litingtung, L. Lei, H. Westphal, C. Chiang, Sonic hedgehog is essential to foregut development. *Nat. Genet.* **20**, 58–61 (1998).
51. E. T. Domyan, E. Ferretti, K. Throckmorton, Y. Mishina, S. K. Nicolis, X. Sun, Signaling through BMP receptors promotes respiratory identity in the foregut via repression of *Sox2*. *Development* **138**, 971–981 (2011).
52. H. Min, D. M. Danilenko, S. A. Scully, B. Bolon, B. D. Ring, J. E. Tarpley, M. DeRose, W. S. Simonet, Fgf-10 is required for both limb and lung development and exhibits striking functional similarity to *Drosophila* branchless. *Genes Dev.* **12**, 3156–3161 (1998).
53. C. Munro, F. Zapata, M. Howison, S. Siebert, C. W. Dunn, Evolution of gene expression across species and specialized zooids in Siphonophora. *Mol. Biol. Evol.* **39**, msac027 (2022).
54. F. Chen, Y. Cao, J. Qian, F. Shao, K. Niederreither, W. V. Cardoso, A retinoic acid–dependent network in the foregut controls formation of the mouse lung primordium. *J. Clin. Invest.* **120**, 2040–2048 (2010).
55. W. Shu, S. Guttentag, Z. Wang, T. Andl, P. Ballard, M. M. Lu, S. Piccolo, W. Birchmeier, J. A. Whitsett, S. E. Millar, E. E. Morrisey, Wnt/β-catenin signaling acts upstream of N-myc, BMP4, and FGF signaling to regulate proximal–distal patterning in the lung. *Dev. Biol.* **283**, 226–239 (2005).
56. T. Okubo, B. L. M. Hogan, Hyperactive Wnt signaling changes the developmental potential of embryonic lung endoderm. *J. Biol.* **3**, 11 (2004).
57. X. Bi, K. Wang, L. Yang, H. Pan, H. Jiang, Q. Wei, M. Fang, H. Yu, C. Zhu, Y. Cai, Y. He, X. Gan, H. Zeng, D. Yu, Y. Zhu, H. Jiang, Q. Qiu, H. Yang, Y. E. Zhang, W. Wang, M. Zhu, S. He, G. Zhang, Tracing the genetic footprints of vertebrate landing in non-teleost ray-finned fishes. *Cell* **184**, 1377–1391.e14 (2021).
58. K. A. Budzik, K. Zuwala, R. Kerney, Tongue and taste organ development in the ontogeny of direct-developing salamander *Plethodon cinereus* (Lissamphibia: Plethodontidae). *J. Morphol.* **277**, 906–915 (2016).
59. B. F. Kingsbury, On the so-called laryngeal tonsils of mammals; with special reference to their structure and development in the cat. *Am. J. Anat.* **72**, 171–197 (1943).
60. G. K. Noble, *The Biology of the Amphibia* (McGraw-Hill, 1931).
61. C. S. Rose, B. James, Plasticity of lung development in the amphibian, *Xenopus laevis*. *Biol. Open* **2**, 1324–1335 (2013).
62. T. Kusakabe, N. Hoshi, S. Kimura, Origin of the ultimobranchial body cyst: T/ebp/Nkx2.1 expression is required for development and fusion of the ultimobranchial body to the thyroid. *Dev. Dyn.* **235**, 1300–1309 (2006).
63. L. Saxén, S. Toivonen, The development of the ultimobranchial body in *Xenopus laevis* Daudin and its relation to the thyroid gland and epithelial bodies. *J. Embryol. Exp. Morphol.* **3**, 376–384 (1955).
64. J. H. Wang, S. J. Deimling, N. E. D'Alessandro, L. Zhao, F. Possmayer, T. A. Drysdale, Retinoic acid is a key regulatory switch determining the difference between lung and thyroid fates in *Xenopus laevis*. *BMC Dev. Biol.* **11**, 75 (2011).
65. M. C. Wilder, The significance of the ultimobranchial body (postbranchial body, suprapericardial body): A comparative study of its occurrence in urodeles. *J. Morphol.* **47**, 283–333 (1929).
66. F. Witzmann, CO_2-metabolism in early tetrapods revisited: Inferences from osteological correlates of gills, skin and lung ventilation in the fossil record. *Lethaia* **49**, 492–506 (2016).
67. J. A. Tihen, D. B. Wake, Vertebrae of plethodontid salamanders from the lower Miocene of Montana. *J. Herpetol.* **15**, 35–40 (1981).
68. R. Kerney, Embryonic staging table for a direct-developing salamander, *Plethodon cinereus* (Plethodontidae). *Anat. Rec.* **294**, 1796–1808 (2011).
69. C. A. Hurney, S. K. Babcock, D. R. Shook, T. M. Pelletier, S. D. Turner, J. Maturo, S. Cogbill, M. C. Snow, K. Kinch, Normal table of embryonic development in the four-toed salamander, *Hemidactylium scutatum*. *Mech. Dev.* **136**, 99–110 (2015).
70. N. Bordzilovskaya, T. Dettlaff, S. Duhon, G. Malacinski, Developmental-stage series of axolotl embryos, in *Developmental Biology of the Axolotl*, J. Armstrong, G. Malacinski, Eds. (Oxford Univ. Press, 1989). pp. 201–219.
71. B. D. Metscher, X-ray microtomographic imaging of intact vertebrate embryos. *Cold Spring Harb. Protoc.* **2011**, 1462–1471 (2011).
72. J.-C. Guimond, M. Lévesque, P.-L. Michaud, J. Berdugo, K. Finnson, A. Philip, S. Roy, BMP-2 functions independently of SHH signaling and triggers cell condensation and apoptosis in regenerating axolotl limbs. *BMC Dev. Biol.* **10**, 15 (2010).
73. R. R. Kerney, J. Hanken, D. C. Blackburn, Early limb patterning in the direct-developing salamander *Plethodon cinereus* revealed by *sox9* and *col2a1*. *Evol. Dev.* **20**, 100–107 (2018).
74. A. M. Bolger, M. Lohse, B. Usadel, Trimmomatic: A flexible trimmer for Illumina sequence data. *Bioinformatics* **30**, 2114–2120 (2014).
75. B. Langmead, C. Trapnell, M. Pop, S. L. Salzberg, Ultrafast and memory-efficient alignment of short DNA sequences to the human genome. *Genome Biol.* **10**, R25 (2009).
76. M. G. Grabherr, B. J. Haas, M. Yassour, J. Z. Levin, D. A. Thompson, I. Amit, X. Adiconis, L. Fan, R. Raychowdhury, Q. Zeng, Z. Chen, E. Mauceli, N. Hacohen, A. Gnirke, N. Rhind, F. di Palma, B. W. Birren, C. Nusbaum, K. Lindblad-Toh, N. Friedman, A. Regev, Full-length transcriptome assembly from RNA-seq data without a reference genome. *Nat. Biotechnol.* **29**, 644–652 (2011).
77. B. J. Haas, A. Papanicolaou, M. Yassour, M. Grabherr, P. D. Blood, J. Bowden, M. B. Couger, D. Eccles, B. Li, M. Lieber, M. D. MacManes, M. Ott, J. Orvis, N. Pochet, F. Strozzi, N. Weeks, R. Westerman, T. William, C. N. Dewey, R. Henschel, R. D. LeDuc, N. Friedman, A. Regev, De novo transcript sequence reconstruction from RNA-seq using the Trinity platform for reference generation and analysis. *Nat. Protoc.* **8**, 1494–1512 (2013).
78. S. Anders, W. Huber, Differential expression analysis for sequence count data. *Genome Biol.* **11**, R106 (2010).
79. S. Götz, J. M. García-Gómez, J. Terol, T. D. Williams, S. H. Nagaraj, M. J. Nueda, M. Robles, M. Talón, J. Dopazo, A. Conesa, High-throughput functional annotation and data mining with the Blast2GO suite. *Nucleic Acids Res.* **36**, 3420–3435 (2008).
80. N. Piekarski, J. B. Gross, J. Hanken, Evolutionary innovation and conservation in the embryonic derivation of the vertebrate skull. *Nat. Commun.* **5**, 5661 (2014).
81. J. D. Steimle, S. A. Rankin, C. E. Slagle, J. Bekeny, A. B. Rydeen, S. S.-K. Chan, J. Kweon, X. H. Yang, K. Ikegami, R. D. Nadadur, M. Rowton, A. D. Hoffmann, S. Lazarevic, W. Thomas, E. A. T. Boyle Anderson, M. E. Horb, L. Luna-Zurita, R. K. Ho, M. Kyba, B. Jensen, A. M. Zorn, F. L. Conlon, I. P. Moskowitz, Evolutionarily conserved *Tbx5–Wnt2/2b* pathway orchestrates cardiopulmonary development. *Proc. Natl. Acad. Sci. U.S.A.* **115**, E10615–E10624 (2018).
82. K. Kishimoto, K. T. Furukawa, A. Luz-Madrigal, A. Yamaoka, C. Matsuoka, M. Habu, C. Alev, A. M. Zorn, M. Morimoto, Bidirectional Wnt signaling between endoderm and mesoderm confers tracheal identity in mouse and human cells. *Nat. Commun.* **11**, 4159 (2020).
83. B. Gerhardt, L. Leesman, K. Burra, J. Snowball, R. Rosenzweig, N. Guzman, M. Ambalavanan, D. Sinner, Notum attenuates Wnt/β–catenin signaling to promote tracheal cartilage patterning. *Dev. Biol.* **436**, 14–27 (2018).
84. K. Sekine, H. Ohuchi, M. Fujiwara, M. Yamasaki, T. Yoshizawa, T. Sato, N. Yagishita, D. Matsui, Y. Koga, N. Itoh, S. Kato, Fgf10 is essential for limb and lung formation. *Nat. Genet.* **21**, 138–141 (1999).
85. M. R. Jones, L. Chong, S. Bellusci, Fgf10/Fgfr2b signaling orchestrates the symphony of molecular, cellular, and physical processes required for harmonious airway branching morphogenesis. *Front. Cell Dev. Biol.* **8**, 620667 (2021).
86. L. De Moerlooze, B. Spencer-Dene, J. M. Revest, M. Hajihosseini, I. Rosewell, C. Dickson, An important role for the IIIb isoform of fibroblast growth factor receptor 2 (FGFR2) in mesenchymal-epithelial signalling during mouse organogenesis. *Development* **127**, 483–492 (2000).
87. M. R. Jones, S. Dilai, A. Lingampally, C.-M. Chao, S. Danopoulos, G. Carraro, R. Mukhametshina, J. Wilhelm, E. Baumgart-Vogt, D. Al Alam, C. Chen, P. Minoo, J. S. Zhang, S. Bellusci, A comprehensive analysis of fibroblast growth factor receptor 2b signaling on epithelial tip progenitor cells during early mouse lung branching morphogenesis. *Front. Genet.* **9**, 746 (2019).
88. P. T. Chuang, A. P. McMahon, Vertebrate Hedgehog signalling modulated by induction of a Hedgehog-binding protein. *Nature* **397**, 617–621 (1999).

89. P. T. Chuang, T. Kawcak, A. P. McMahon, Feedback control of mammalian Hedgehog signaling by the Hedgehog-binding protein, Hip1, modulates Fgf signaling during branching morphogenesis of the lung. *Genes Dev.* **17**, 342–347 (2003).
90. J. C. Grindley, S. Bellusci, D. Perkins, B. L. Hogan, Evidence for the involvement of the *Gli* gene family in embryonic mouse lung development. *Dev. Biol.* **188**, 337–348 (1997).
91. J. Motoyama, J. Liu, R. Mo, Q. Ding, M. Post, C. C. Hui, Essential function of *Gli2* and *Gli3* in the formation of lung, trachea and oesophagus. *Nat. Genet.* **20**, 54–57 (1998).
92. S. Kimura, Y. Hara, T. Pineau, P. Fernandez-Salguero, H. C. Fox, J. M. Ward, F. J. Gonzalez, The T/ebp null mouse: Thyroid-specific enhancer-binding protein is essential for the organogenesis of the thyroid, lung, ventral forebrain, and pituitary. *Genes Dev.* **10**, 60–69 (1996).
93. S. Kimura, J. M. Ward, P. Minoo, Thyroid-specific enhancer-binding protein/thyroid transcription factor 1 is not required for the initial specification of the thyroid and lung primordia. *Biochimie* **81**, 321–327 (1999).
94. R. Arora, R. J. Metzger, V. E. Papaioannou, Multiple roles and interactions of *Tbx4* and *Tbx5* in development of the respiratory system. *PLOS Genet.* **8**, e1002866 (2012).
95. J. Que, T. Okubo, J. R. Goldenring, K.-T. Nam, R. Kurotani, E. E. Morrisey, O. Taranova, L. H. Pevny, B. L. M. Hogan, Multiple dose-dependent roles for *Sox2* in the patterning and differentiation of anterior foregut endoderm. *Development* **134**, 2521–2531 (2007).
96. M. Teramoto, R. Sugawara, K. Minegishi, M. Uchikawa, T. Takemoto, A. Kuroiwa, Y. Ishii, H. Kondoh, The absence of *SOX2* in the anterior foregut alters the esophagus into trachea and bronchi in both epithelial and mesenchymal components. *Biol. Open* **9**, bio.048728 (2020).
97. J. Que, M. Choi, J. W. Ziel, J. Klingensmith, B. L. Hogan, Morphogenesis of the trachea and esophagus: Current players and new roles for noggin and Bmps. *Differentiation* **74**, 422–437 (2006).
98. E. D. Dickman, C. Thaller, S. M. Smith, Temporally-regulated retinoic acid depletion produces specific neural crest, ocular and nervous system defects. *Development* **124**, 3111–3121 (1997).

Acknowledgments: We thank M. Aja, B. Cooke, J. Dorantes, C. Eng, M. Hawkins, A. Koomas, M. Laslo, H. Maddin, J. Martinez, M. McCarroll, N. Piekarski, A. Sahay, A. Saunders, E. Sefton, S. Tilley, D. Woolf, J. Wu, and Y. Wu for assisting with field collection of embryos; H. Müller, J. Larson, and H. Maddin for assisting with μCT scanning and image reconstruction; C. DeVane and A. Everly for overseeing live animal care; and K. Adler (Cornell University) for obtaining for us a copy of G. Mekeel's unpublished Ph.D. dissertation. **Funding:** This work was supported by the NSF Graduate Research Fellowship (Z.R.L.); NSF grants DBI-1702263 (J.H.) and EF-0334846 (J.H.); Museum of Comparative Zoology, Harvard University, Kenneth Miyata Grant (Z.R.L.); Museum of Comparative Zoology, Harvard University, Robert G. Goelet Summer Research Award (Z.R.L.); and Museum of Comparative Zoology, Harvard University, Wetmore-Colles fund (J.H.). **Author contributions:** Designed and carried out experiments: Z.R.L. and J.H. Histology: Z.R.L. and R.K. μCT scanning: Z.R.L. and R.K. Gene cloning: Z.R.L. and R.K. Data analysis: Z.R.L. and R.K. Writing—original draft: Z.R.L. Writing—review and editing: Z.R.L., R.K., and J.H. **Competing interests:** The authors declare that they have no competing interests. **Data and materials availability:** All data needed to evaluate the conclusions in the paper are present in the paper and/or the Supplementary Materials. In addition, three datasets from a micro–computed tomography (μCT) scan of an embryo of the red-backed salamander, *P. cinereus*, are publicly available from Harvard Dataverse (https://doi.org/10.7910/DVN/SKN3SM, https://doi.org/10.7910/DVN/VRHMIO, and https://doi.org/10.7910/DVN/FFW266), and genetic data are publicly available from the NCBI Sequence Read Archive (https://trace.ncbi.nlm.nih.gov/Traces/sra/?study=SRP357481 and www.ncbi.nlm.nih.gov/bioproject/PRJNA802070).

Submitted 14 February 2022
Accepted 1 July 2022
Published 17 August 2022
10.1126/sciadv.abo6108